Developing General Purpose Apps to Automate Image Analysis of Wave-Augmented-Varicose-Explosion Atomization and other Multi-Phase Interfacial Flows

Ethan Newkirk

A Senior Thesis submitted in partial fulfillment
of the requirements for graduation
in the Honor Program
Liberty University
Spring 2024

Acceptance of Senior Honors Thesis

This Senior Honors Thesis is accepted in partial
fulfillment of the requirements for graduation from the
Honors Program of Liberty University.

_____

Wayne Strasser, Ph.D., P.E.
Thesis Chair

_____

Ola-Lekan Shobayo, Ph.D.
Committee Member

_____

Chris Nelson, MFA
Assistant Honors Director

_____

Date

Abstract

Atomization involves disrupting a flow of contiguous liquid into small droplets ranging from one submicron to several hundred microns (micrometers) in diameter through the processes of exerting sufficient forces that disrupt the retaining surface tensions of the liquid. Understanding this phenomenon requires high-speed imaging from physical models or rigorous multiphase computational fluid dynamics models. We produce a MATLAB application that utilizes various methods of image analysis to quickly analyze and store mathematical data from detailed image analyses. We present a user with numerous tools and capabilities that provide results that deviate from 1.8% to 8.9% of the original image sequence depending on various factors. After comparing two-dimensional axisymmetric and planar cuts with the three-dimensional flat rendering, we found that the data is more dissimilar than similar based on analysis of mean, standard deviation, maximum, and minimum measurements.

Keywords: computational fluid dynamics, atomization, droplets, waves, image analysis

Developing General Purpose Apps to Automate Image Analysis of Wave-Augmented-Varicose-Explosion Atomization and other Multi-Phase Interfacial Flows

Atomization, which breaks apart a liquid into droplets, is valuable to many applications within the fields of medicine, meteorology, printing, and many others, which make use of sprayers or nozzles. Certain sprayers or nozzles are designed to feed a liquid into a stream of fast-flowing gas, accomplishing the disruption of flow that characterizes atomization. While there is extensive research on the topic of atomization, there remains a gap when addressing a three-dimensional representation of the effects of the atomized flow downstream from the nozzle. Current technology has allowed researchers to perform computer simulations that produce a two-dimensional reproduction of the subsequent behavior of a chosen liquid after disruption. The field of fluid mechanics which specifically seeks to investigate and numerically analyze those simulations to understand fluid flows is a branch termed computational fluid dynamics (CFD).

The field of CFD is vast, accounting for thousands of intricate studies that seek to investigate the physics behind various fluids. Atomization is one particular focus that incorporates many differing research paths and fields of study. Lefebvre (2011) describes the phenomenon “as a result of the competition between the stabilizing influences of surface tension and viscosity and the disruptive actions of various internal and external forces” (para. 4). Within the path of studying atomization, there are no prominent tools for quickly measuring the breaking apart of fluids simulated by many researchers. Specifically, we are interested in measuring processes where an inflow of slurry through a nozzle is motivated to take the form of a wave as a result of external gas forces exerted on the liquid. We simulate where a puree is

injected into a steam flow which causes the formation of waves inside the nozzle that periodically build, reach an apex, and then burst at a high frequency. This specific observed phenomenon has been coined as “Wave-Augmented-Varicose-Explosions” (WAVE) by Wilson, Strasser, and Prichard (2023, para. 4). There is a considerable gap remaining in understanding this WAVE atomization and detailing the three-dimensional attributes of the waves formed along the three-period wave cycle. WAVE simply describes three attributes including:

> 1) The momentum of the crashing wave creates radial bulges in the liquid film, bursting droplets outward at regular intervals. 2) The high blockage ratio of the wave causes an intense pressure increase behind the wave that assists the wave momentum in driving liquid film rupture and slurry disintegration. 3) The extension of the slurry as a wave into the steam flow increases the interfacial area, providing more space for the steam to peel off droplets (Wilson et al., 2023, p. 7).

CFD Contour Plots

CFD simulations can be used to produce estimations of this fluid movement, where desirable attributes can be tweaked and optimized after interpreting the data. External factors such as nozzle shape and size, inflow gas, and liquid velocity can be changed to further induce atomization of the chosen liquid. Contour plots (colored images) are one valuable output from CFD simulation tools which are the focus of analysis for this research. These plots are imaged representations of the simulated flow character. Contour plots provide excellent models, but sometimes it is necessary to analyze thousands of contour plot images for specific physical properties. However, the processing of massive data sets from these simulations can be heavily

time-consuming. As Dang et al. (2020) write, “It is desirable to develop screening approaches that can utilize small quantities of liquid fuels and rapidly evaluate physical and chemical properties of relevance” (p. 2). Therefore, there remains a need for a rapid method of evaluating the properties of relevance to increase the performance of atomization.

Purpose

As researchers Sikka et al. (2021) reflect on in terms of the shifting focus of waves, “lately, the annular sheet has also received some attention” (p. 1). We find that MATLAB contains a plethora of image analysis tools that aid the analysis of WAVE and other multiphase interfacial flow atomization. MATLAB includes a downloadable image analysis toolbox that holds various basic tools for performing the aforementioned analysis of images. These can be constructed in loops to create a function applicable to performing calculations of fluid simulation image data stores. MATLAB also contains an app designer database which gives the user control of a skeleton application along with buttons and other functionalities that can be applied. The research herein involves utilizing MATLAB to write functions in the app designer to program an application to automate image analysis of imported fluid simulations. This leaves many questions that drive the progress and aim of the research from here. What methods are necessary to conduct image analysis of these simulations? What measurements can be performed on these images from contour plots using MATLAB? Can we patch together different cuts of two-dimensional simulations to effectively create a three-dimensional representation of the flow character?

With the knowledge readily available in the field of CFD and image analysis, the developed application within MATLAB will be tested based on the effectiveness of calculating measurements of different contour plots. These tests will be evaluated and applied to determine

the similarity between data structure and grouping of three main directories of contour plots. The goal of this research is the analysis of WAVE atomization computer-generated reproductions in addressing with greater expertise the wave oscillation in the nozzle. More specifically, we aim to uncover whether two-dimensional planar and axisymmetric contour plots can estimate the three-dimensional WAVE behavior. We will begin with a background of fluid atomizers, image analysis, and batch processing, a methodology of MATLAB application construction, results of the application's processing of CFD directories, a discussion of findings and application limitations, a conclusion of the findings, and future implications in the field of fluid mechanics. Gaining better knowledge of this phenomenon will help to aid in the further optimization of countless fluid systems through the computation of the underlying physics. Bridging this gap in research is necessary to build upon for uses across a plethora of fields involving any usage or manipulation of the properties and behavior of a fluid.

Background

Fluid Atomizers

The image analysis herein focuses on looking into multiphase flows including bubbles, droplets, atomizers, sprays, and bubble columns. The phases of liquid atomization occur a multitude of times, requiring evaluation of each wave formation to construct a full picture of the shearing liquid. Lefebvre (2011) writes that "numerous spray devices have been developed which are generally designated as *atomizers*, *applicators*, *sprayers*, or *nozzles*" (para. 2). The interactions of the multiphase flows in atomizers allow for the breaking apart of a continuous liquid for adaptive purposes. These devices can then be purposed to provide benefits to a variety

of fields of research, including medicine, meteorology, and printing. Researchers Akinyemi et al. (2023) write that:

> liquid jets and/or sheets are discharged immediately at the atomizer exit in the conventional AB [air-blast] and PS [pressure swirl] atomizers and break up into shorter ligaments as the result of the primary atomization, and these disintegrate into droplets further downstream, defined as secondary atomization (p. 2).

The simulation of atomization utilizes certain forces and shapes to control the spray. This is accomplished by optimizing various properties of the atomizer, liquid, and feed gas. In particular, two separate feeds, one carrying a low-velocity inflow of liquid and the other a high-velocity inflow of gas, are directed toward one another in such a way as to induce interaction. Jackiw and Ashgriz (2022) explain that the main forces of study are "how the liquid jet initially interacts with the co-flowing air jet and how this interaction leads to the breakup of the liquid jet under the aerodynamic forcing of the gas flow" (p. 18). The resulting waves are analyzed throughout multiple recurrent phases, or oscillations of waves, which see the formation and disruption of a contiguous liquid fed to the atomizer. Lefebvre (2011) also explains that "the liquid properties of importance in atomization are surface tension, viscosity, and density" (para. 4). As such, our application will measure and compare the frequency of oscillation and wave height over time of fluid plume simulations evaluated from various cuts.

Image Analysis

From these CFD contour plots, two-dimensional frames can be extracted for individual study. Image analysis of these frames remains the primary approach for calculating dynamics of concern in the flow setup. It is thus very important to be able to address and compute desirable

sections of flow. “Image analysis and post-processing are used to estimate the decay rate and frequency of the oscillation, which are subsequently used to calculate fuel surface tension and viscosity” (Dang et al., 2020, p. 2). Thus, image analysis primarily revolves around the preparation of images for later analysis by applying multiple steps of data isolation, leading to the measurement of sections in the image. These methods can be automated to replicate calculations on thousands of frames, gathering data integral for shaping the resulting liquid breakup. This automation can be accomplished via batch processing utilizing artificial intelligence or explicit programming language.

Batch Processing

Batch processing is a method aimed at performing simultaneous analysis and calculation of images either through parallel processing or linearly stepping through directories image-by-image. Both methods of batch processing save immense time when analyzing large amounts of images. As Mostert et al. (2022) write in their research:

> wave breaking involves transition from two-dimensional (2-D) laminar wave flow to three-dimensional (3-D) turbulence … despite the essentially 3-D nature of the turbulence resulting from breaking, 2-D breakers at the tested conditions have provided a reasonable estimate of the dissipation rates obtained from experiments and 3-D computation (p. 2-3).

Similarly, we aim to estimate the behavior of 3D WAVE breakup from 2D visual data slices of the complete 3D simulations of annular flow atomization via batch processing. Artificial intelligence allows for base code to be amended without alteration by a human programmer, thus a program independently updates its code from experience. For the focus of the research here, we

will utilize only explicit programming for the design and structure of batch-processing image analysis.

Methodology

CFD Simulations

The main methodology of fluid mechanic research is accomplished via physical modeling and high-speed camera rigs or computer simulations that require processing over several months. Researchers Choi et al. (2022) explain that "Overcoming the difficulties and lack of analytical explanation of such chaotic atomization phenomena, we were able to identify four different atomization regimes (backflow, bulk atomization, droplet atomization, and floating liquid column)" (p. 37). After their findings, they also reflect the lack of analytical systems that reflect both the visualization and measurement of experiments with annular atomizers. As researchers perceive the effects of atomization in four regions of the flow character, each section adds to the overall understanding of phenomenon characteristics. Therefore, the unique value of the ability to produce and measure two-dimensional slices automatically proves to be a need in the field.

From the slices created, we can then analyze the specific properties of each region of the atomized fluid. An arsenal of tools is available through MATLAB's databases, including the Image Analysis Toolbox. From this comes a package of many valuable functions which can be used for image preprocessing steps. MATLAB also includes a valuable feature that allows for the manipulation of skeletal application creation. Through these tools, an application for image analysis can be constructed providing quick automation of frame preprocessing and batch processing that can be used in this problem solution. Researchers Minko et al. (2021) reflect the current difficulty and lack thereof in "performing a large number of parametric calculations

[that] requires significant computing resources which complicates the operational solution of several practical problems" (p. 2). We begin by acquiring frames of the contour plot simulations, preprocessing these to prepare them for measurement, building other capabilities to isolate desirable sections of WAVE flow, and writing loops to calculate the section's heights over time.

Image Acquisition

Two-phase fluid simulations require a vast amount of computing power, often achieved via the resources of a supercomputer. Often, these computers are utilized to produce contour plots or imaged representations of the mechanics and effects of atomization. The contour plots display "slurry volume fraction (VF)" (Wilson et al., 2023, p. 9). See Figure 1. The resulting plots provide useful data in visualizing the velocities of sections of the fluid bulk for determining where sections of atomization begin to occur. While these plots offer much valuable insight into the physics of the conditions of liquid shearing, they result in vast data sets. These sets must be evaluated to extract the underlying measurements of certain properties, but the sheer size of the data is overwhelming. Khalid et al. (2017) write that "generally, the simulation in ANSYS FLUENT involves three main stages which are pre-processing, solver and post processing" (p. 2). Thus, the production of three-dimensional models slows down the possible progress that could be made in multiphase flows. Understanding the three-dimensional properties of waves is necessary, as variation along the entire annulus of the wave is observed. However, solving two-dimensional axisymmetric and planar versions of the full three-dimensional CFD

Figure 1

Note. Yellow is the wave to be studied.

(Wilson & Strasser, 2022)

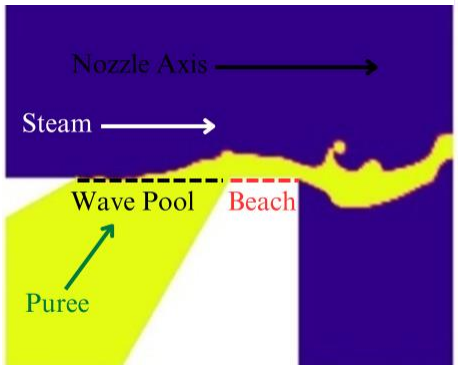

simulation induces potentially significant errors in the CFD simulation and resulting image analyses. By judicious application of our image analysis tool, we aim to precisely define how much error occurs from approximating 3-D atomization as 2-D. Both 3-D and 2-D produce similar styles of images. However, a 3-D image is only an infinitesimally small slice of the modeled region. 2-D images represent the entirety of the simulated domain, and the hope is that the results will be similar, as 2-D computing requires orders of magnitude less computing time.

Three CFD Directories

While programs currently exist that enable a human user to measure various parts of the images in these sets, repeating this process across hundreds or thousands of frames is heavily time-consuming. These two-dimensional measurements can be pieced together to give more information on the mechanics of the process of shearing the liquid. The current state of technology allows for the automation of computer computations, which can be constructed to automatically analyze specific parts of the images over the entire data set. By automating the process of mathematical measurements on each frame, researchers have greater freedom to make alterations to the tools of atomization to optimize the sprayer. We have acquired three main directories of various atomization simulations of differing scaling including an estimated 1,000 frames each. These include 2DA, 2DP, and 3D which will be measured through computer automation in the MATLAB Image Analysis application. Researchers Zaidi et al. (2020) also made use of MATLAB for processing their imaged representations of focus to distinguish the foreground and background. The comparison of these two-dimensional slices with the three-dimensional annular counterpart will prove or disprove the ability to simplify mathematical measurements.

MATLAB Application Features

Image Preprocessing

The effective process for measuring the properties of the contour plots requires image analysis of each frame and manipulation of the images to isolate the desired portion for measurement. Before we can measure the desired properties of the waves, the image must go through preprocessing to best prepare it for accurate results. Many processes of noise reduction, smoothing, segmentation, edge removal, opening, closing, and hole filling, among many others are applied as required to the image during this step of image analysis. The tools used within the application developed herein through MATLAB include segmentation, edge smoothing, cropping, connectivity averaging, and averaging filters. Researchers Oswald et al. (2019) used similar MATLAB steps in increasing contrast in the image, adaptive threshold method (binarization), and small object removal. This preprocessing step is necessary to conduct before the image is analyzed through automation; otherwise, the data is not easily extracted or correctly represented. This phase of prepping the individual frames for analysis separates the object of focus in the foreground from that which should not be measured in the background. However, it is often difficult to distinguish the unique characteristics of the desired portion of the simulation from the surrounding image. Thus, many steps are taken to ensure accurate contrasts that properly represent the original image. Once the preprocessing phase is complete for test subjects of the contour plots, we apply the methods of image analysis to each frame through automation before performing measuring steps.

The full range of image analysis steps and methods are performed by the Image Analysis Wave Atomization application in MATLAB we write for this research. Each section within the

app allows for manipulation and custom analysis for a variety of atomization datastores. Alternatively, researchers Radcliffe and Reklaitas (2021) comment that their process within MATLAB began with "(1) load images, edge detection in parallel; (2) single CPU object tracking/event recognition, and then (3) save results," allowing them to automate the programs' capability of automatically recognizing sections of the flow (p. 18). However, the focus herein intends to compare the frequency of bulk fluid height as observed in the WAVE simulation. A column will be selected in the contour plot frames which records height values as the fluid passes through. This data will be scaled and converted to export a CSV file of numerical information, such as the height of the column of interest. Primarily, the entire breadth of interest lies in the resulting behavior of the liquid as it passes over the beach shelf while exiting the atomizer nozzle. This beach sees the interaction between the inflow of high-velocity gas with the slow inflow of slurry, thus the causation of shearing of a contiguous liquid. If image preprocessing can prepare each frame for proper measurement of the beginning stages of atomization, the axisymmetric and planar slices of the three-dimensional annular simulated flow can be compared. The axisymmetric section of the three-dimensional model contains a slice that is symmetrical when rotated around the axis of interest and neglects any change in atomization (or wave, in this case) character around the atomizer's circumference.

Segmentation

The first step in achieving proper analysis of the output frames is applying multiple image preprocessing methods to isolate the desired data in each image. A basic knowledge of the way that images are stored digitally aids our ability to perform image analysis. All color images are stored as a matrix of intensity values across three slices of red, green, and blue. Each color

matrix contains intensity values ranging from 0 to 255 which measure the amount of the color in each pixel. These three individual color matrices are then overlayed to produce the images that are seen. Segmentation involves isolating a set range of pixel values to convert the image to binary data of 0's and 1's. It makes use of the contrast naturally found between subjects within an image that occurs with differing amounts of each matrices' intensity histogram. The first step of segmentation involves converting an RGB image to grayscale. This grayscale image exists as a singular matrix of intensity values from 0 to 255 which instead determines the amount of black (closer to 0) or white (closer to 255). Additionally, the grayscale form of the original collapses the three-color matrices into one, making the file smaller in size and therefore more efficient for processing later. The result is an image consisting of a range of white, gray, and black colors. Plotting a histogram of the pixel intensity values found in the grayscale version allows the user to visualize where groupings of data retain their values. We can thus estimate what range of intensities are included in a part of what is seen in the image, such as the wave. From this, we can restrict the grayscale image to a range of pixel values, thus converting each pixel to Boolean data. If the pixel is within the range of intensity values, it is assigned a 1 or true value, and if it falls outside the defined range, it is assigned a 0 or false value.

Within the MATLAB app we wrote, after selecting an image datastore from which the frames are taken and contrasted, an example frame is taken from the datastore input and can be plotted by clicking on the "Plot Value Histogram" button on the interface. The button executes code which creates a bar graph with the number of pixels with each of the intensity values in the range of 0-255. This is accomplished through MATLAB's "histogram" predefined function from the downloadable image analysis toolbox mentioned beforehand. Jungst et al. (2022) wrote about

MATLAB “operator [which] determines the magnitude of the intensity gradient at each pixel. Then, the image is binarized by thresholding at a gradient magnitude value of 0.03, which visually yielded good results” (p. 6). After observing the distribution of pixel intensities, we can define a lower and upper threshold from which to determine the segmentation isolation. See Figure 2. With these values, we create a conditional statement of *app.firstBW = firstGS>app.Low & firstGS<app.High* to exclude any values not within the chosen *app.Low* and *app.High* values are selected in the Lowest Value and Highest Value numeric prompts within the Segmentation Thresholding section of the app. Capability also exists for testing the chosen segmentation values by clicking the “Test Segmentation” button. Upon a user’s click, the button executes the conversion to grayscale of a singular image in the selected directory and thresholding chosen and displays a binary image of the result. The binary image contains two colors which indicate the foreground (in white) and the background (in black). The foreground contains any true pixel which will be measured in the batch processing, while the background is entirely ignored. From this, a user can make necessary changes to isolate the data desirable for evaluation. This step allows the user to verify that segmentation is applied to the correct sections of the images and that no intended data is left out of focus.

Figure 2

Application Interface

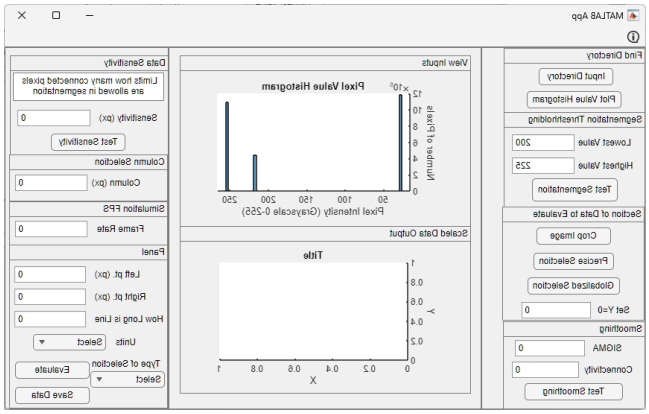

Smoothing Edges

Some exported simulation slices lack detail, resulting in jagged and pixelated edges. This is the result of exporting contour plots in lower quality, often through the intentionality of reducing file sizes for vast arrays. Radcliffe and Reklaitas (2021) communicate the pre-existing problem that is caused by "the quality of edge maps is dependent on both image quality and the edge detection algorithms used; if image quality is lacking, then more elaborate schemes are required to produce satisfactory edge maps" (p. 18). Before the frames can be segmented and measured, the edges need to be smoothed to achieve accurate results that will not be skewed. Many current mathematical processes exist that offer varying results in averaging the jagged edges to the line of best fit as seen in the general shape of the wave. Many predefined MATLAB functions make quicker work of this complicated preprocessing step and include the Gaussian filter, histogram equalization, structuring element shape defining, and eroding functions. After a frame is converted to grayscale, we apply a Gaussian filter to the image. The "imgaussfilt" function within MATLAB takes in parameters of a grayscale image and has additional options for determining the strength of the Sigma value. This Sigma parameter essentially defines the amount of bell-curve spread of the Gaussian filter, affecting the amount that blurring is applied to an image. A Gaussian filter effectively blurs the image input and allows for the edges of a section of the image to be smoothed out as a result. The ability to define the strength of the Sigma parameter in the function alters the intensity of the blurring applied to the image. Here, we use the grayscale image with a Sigma value of 7 to begin the Gaussian filtering process. This initial filter causes the intensity values of pixels mentioned beforehand to be spread out farther, necessitating some level of equalization to achieve proper contrast. This indicates initial testing results with a higher level of blurring applied, thus altering the original values. Later, we will test

various filter strengths to determine the effect on the distribution of data from an un-smoothed original frame of reference. The contrast between groupings of pixel intensity values helps in the binarization step, causing the Boolean image to not include unwanted sections of pixels.

Another useful predefined function within MATLAB's image analysis toolbox includes histogram equalization. The function used is called "adapthisteq" and calls one parameter of a grayscale image, along with further customization of determining the equalizing distribution shape. The Rayleigh shape is chosen here, resulting in intensity values that have an increase in contrast between groupings. Once the grayscale image has gone through Gaussian filtering and equalizing, it can enter the refining step of binarization. Looking at a histogram of the new grayscale image helps determine which threshold of values to use in filtering the image. Through this, the result is a Boolean image of 0's and 1's, effectively creating a black-and-white image, where white represents true values and black represents false values.

Unwanted Data Removal

Often, some droplets produced from the fluid shearing are unnecessary for mathematical analysis and should not be factored into the entire picture. Image analysis provides tools for removing certain groupings of data that do not meet specific requirements. When studying the overall bulk of liquid passing through the atomizer, individual droplets that occur downstream in secondary atomization are unnecessary. MATLAB's "bwareaopen" predefined function in the Image Analysis Toolbox allows the user to specify parameters such as connectivity, which searches the image for any grouping of foreground pixels that are smaller than the parameter. The function executes pixel-by-pixel analysis over the entirety of the image and compares the total area of the connected foreground with the defined connectivity. Researchers Jungst et al.

(2022) used a similar method to remove data that inhibited accurate results for the region of bulk atomization in which “to counter this bias, features in which the number of Sobel-edge pixels are below a size-dependent minimum are discarded” (p. 59). We determined a base size-dependent minimum of 650 pixels to be effective in removing the foreground droplets that were segmented in earlier operations.

Although the image is in the final form that allows proper height measurements, the steps used throughout the smoothing progress often produce additional unwanted lines and bubbles. This is the result of averaging the values of intensity, meaning that the thresholds defining the Boolean image include some unwanted sections of the image. This includes two lines, one vertically oriented to the right of the wave and the other horizontally above the wave. To deal with this, a structuring element shape can be defined and then applied to the image in morphological operations including either erosion or dilation of the image. These operations determine if the foreground should become the background and vice versa. Erosion causes a sweep of the entire picture, where the minimum value of a structuring area is taken, causing the resulting foreground total area to be smaller. Dilation causes a sweep of the picture pixel by pixel and takes the maximum value of the structuring shape area, increasing the foreground area. Thus, to smooth out stair-step edges, we performed an opening process, which performs erosion and then dilation. The opening process is defined in MATLAB’s “imopen” function, producing an increase in the total foreground near the areas previously dense in true values. Zhang et al. (2022) “applied to decrease the size of particles of processed image” (p. 654). We therefore define a structuring element with a disk shape and connectivity of 7 pixels and apply it to the image in an eroding process. The “imopen” function in MATLAB takes parameters of a binary

image and structuring element shape and erodes the image row by row and column by column. Additionally, an ANYS logo remains in the upper right corner of the contour plot, even after the morphological opening. We found that combining the morphological operations in addition to redefining the connectivity minimum to around 1750 pixels resolved this issue. See Figure 3. After this final step, we have a frame from the contour plots which can be measured for wave height over time.

Additional Capabilities

Occasionally, cropping and various types of column selection are desirable for further isolation and increased resolution of the region of interest. We wrote the "Section of Data to Evaluate" panel within the app to accomplish this. Cropping a frame's external boundaries creates a zoomed-in focus which can eliminate the outer edges of the image subject that are difficult to separate from the intended foreground when segmenting. Additionally, in future application updates, choosing to crop an image to a set boundary will allow a section-wise height measurement to be performed as opposed to the typical column-wise measurement. This section-based binary calculation will be able to extract the wave's greatest pixel height over a length of x-values. Precise and global selections provide differing opportunities for determining the best area of evaluation. The precise selection takes the user's crop area and applies it to a binary image from the directory, thus displaying a close-up image of

Figure 3

Minimum Connectivity

Note. Green indicates data that was removed

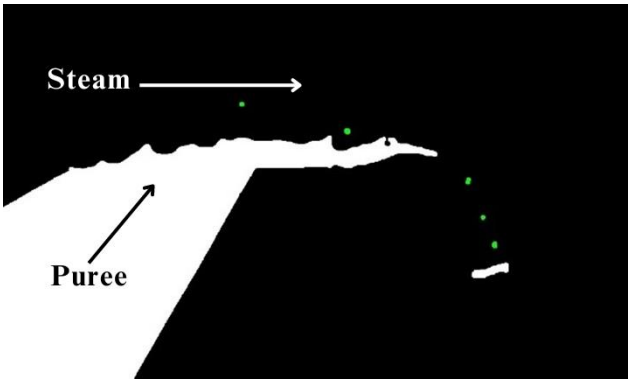

one of the frames. The global selection is useful when comparing results across a multitude of directories for comparison, therefore allowing an uncropped frame display for area determination. Finally, the option to define a new y-axis zero allows for the cutting off of potential values that may be picked up along the processing alternatively. Not only so, but many contour plots are plotted upside down when looking at y-values, thus complicating a grid-based measurement system's results when processing. As such, when a new y=0 value is defined at the lowest point of measurement interest, the axis can be flipped and provide grid coordinates from which we can evaluate the height.

If a user selects the "Crop Image" button from the panel, the app executes a predefined "imcrop" function from MATLAB's toolbox, creating a cursor-drawn rectangle selection. With a displayed frame that is overlayed by a grid with x and y coordinates, a user can drag and move a selection box for desired cropping. The length and height of the selection box, once cropped, are stored in global variables that are stored for later batch processing.

The Precise Selection button is chosen after cropping a frame and displays a binarized image from the directory that has been cropped to the predetermined area. This figure is overlayed with x and y coordinates and contains many prewritten tools along the top ribbon as defaulted with MATLAB's app designer capabilities. The user can then use various tools in the ribbon to select precise coordinates to keep differing directories under the same scaling, along with finding the edges of sections to be measured. Alternatively, the Global Selection button displays an RGB frame with x and y coordinates in a figure with the same default ribbon of tools. This selection is used to determine global values of reference to be compared between if correlating the data produced from multiple directories of frames.

While most choices beforehand are optional to interact with the functioning of the app's design, the y=0 numeric dialogue box is required for proper results. When utilizing either precise or global selections, the user makes note of the lowest y-coordinate in the desired regime of the WAVE flow. This input box stores a global variable that is extracted later during the batch processing phase and cuts off all values below the new y=0 shelf, thus allowing for a maximum true value pixel to be recorded. Once the y=0 is determined, the axes are flipped to account for the rotation of axes that is found often when taking slices of three-dimensional models.

Wave Measurement

Now that the necessary image analysis pre-processing steps have been developed to prepare the image, only viable data remains. As a result, the batch processing of thousands of individual frames is much easier to compute and eliminates certain possible errors that can occur behind the scenes when a computer runs code. For the height of the bulk wave to be addressed, rudimentary functions allow us to measure the difference between the apex of the wave and the shelf which motivates the primary puree atomization. To do this, we isolate the column that the user chooses in the earlier steps, extracting all coordinates from any true pixels (value of 1) within the column. We then store the max y-value from the matrix of all true pixel coordinates as the height of the wave. This y-value remains the correct measure of the effective height of the liquid at this x-wise column selection, as the redefining of the y=0 shelf earlier begins at the lowest point of possible wave formation. The height is initially stored in pixels, which are later converted to alternative units of measure.

All individual steps previously established are performed as needed on an individual frame and must be applied linearly to function properly. The user must determine: 1) Which

section of wave to evaluate. 2) Whether global or cropped analysis is more beneficial. 3) The new y=0 value to define. 4) The amount of smoothing to apply and if necessary. 5) How sensitive the measurement should be. 6) Which column of the wave to measure. 7) What will be used to define a relative measurement. Thus, automation for the image preprocessing and measurement of the directories is desired to apply all manipulations to each frame in a directory as quickly as possible. This is achieved through batch processing, a process that can equip nested loops for performing all necessary image pre-processing, segmentation, and measurement.

Many loops can be linked together in a nested fashion to automate each image's necessary alterations, including later height evaluation. The nesting of multiple *if-else* and *for* loops gets complicated quickly and requires particular attention to ensure the structure performs as intended. See the numbered list below for the visualized nested loop structure. Here, we define the structure as an *if-else* statement where if the user chooses global selection, loop 1 is executed; otherwise, loop 2 is entered. The *if* (loop 1) performs all processing without cropping of frames. Within the *if* statement we execute a *for* (loop 1.a) that increments the value of a variable *i* from 1 to the total number of images stored in the directory with each pass, entering another *if-else* statement defined by whether the user changes the Sigma value or not. In this sub-parameter (1.a.i), if the user decides to change the Sigma value, the *i'th* file in the directory goes through the smoothing process outlined earlier. The sub-*else* statement (1.a.ii) executes if the user does not change the Sigma value, in which basic segmentation is applied. The larger *else* (loop 2) executes if the selection is not global and nests another *if-else* statement within a *for* loop (2.a) executing based on whether the Sigma value has been changed. As with the other nested *if-else* statement, if the Sigma value has been changed (2.a.i), the cropped frame goes through

smoothing. If not, the else statement (2.a.ii) applies basic segmentation to the cropped frames without cropping. Before the nested loops, we pre-allocate an empty array determined by the size of the directory that was input, which helps speed up the overall processing time. Before the end of each nested loop, we scale the units measured in pixels to mm and store the value in the associated cell within the pre-allocated array. Here, we give a bulleted list following the looping structure explained above which performs the image analysis batch processing:

1. *if* global selection is used
    a. *for* i: number images in directory
        i. *if* user chooses a Sigma value
            1. perform smoothing and global measuring
        ii. *else*
            1. perform global analysis
2. *else*
    a. .for i: number images in directory
        i. *if* user chooses a Sigma value
            1. perform cropping, smoothing, then cropped measuring
        ii. *else*
            1. perform cropping then cropped measuring

From this, every frame's resulting height can be referenced to the passage of time pertinent to each simulation and then scaled for the proper time axis that compares each of the three directories equally. Each .tif image in the 2DP, 2DA, and 3DGB90 respectively is sorted based on the time stamp recorded at the end of the file name. From these time stamps, we can determine the total amount of time passed between the first and last frames. It was found that 2DA recorded waves over 0.015 seconds, 2DP over 0.020 seconds, and 3D over 0.007 seconds, so we must establish an appropriate time axis to plot all height results. Thus, the end of the nested loops executes a plotting of the full array chosen earlier in the process, containing the height of the wave in each frame in millimeters. The graph is for the data to be visualized with an x-axis of seconds passed and a y-axis of the height of the bulk fluid wave. The x-axis and y-axis

of the final plot of wave height (in this case) versus time are not to be confused with the x-axis and y-axis of the images.

Verification and Validation

Before sorting through and interpreting the results, it was necessary to ensure the accuracy of height measurement methods and all loops in the batch processing that execute the user's choices. To validate the data measurements produced by the application and batch processing loops, we performed various verification tests to evaluate the accuracy of the application's results when compared to the original, unedited images. One of the main questions demanding answers regards the possible skewing of data based on alternate beach orientations. These differences can occur as a result of producing simulations at various focal points, causing the shelf to be higher or lower in the image. Though we never define the application to gauge wave height based on ordinate orientation, small discrepancies in code can result in measurements not intended. We began accuracy verification by gathering five random frames from each of the three directories, on which we performed no segmentation or pre-processing, but rather kept in original RGB condition. Each of the five frames was manually measured at a global location relative to the focal point used in the simulation directory. This manual column mimicked the equal location of column measurement used previously in the application. These heights were compared to data from the same five frames run through the application where the same section of wave was evaluated. After scaling, we produced data that was nearly 0% different than that of the manual analyses. Thus, it was determined that there was no skewing of the heights measured from the application's segmentation, preprocessing, and batch-processing methods.

Results

Segmentation Accuracy

Segmentation methods of isolating pixel intensity values between a certain range are often effective but can leave out desired information in the picture. However, the segmentation remains of high accuracy. Monieta shares that:

> contrast ratio measures are based on measuring the difference between dark and light intensity points of local image patches. However, the contrast ratio is influenced by the surrounding local contents (i.e., the local distribution of pixel values) … determined by employing a global analysis of the blackening degree of gray images and the share of basic RGB (red, green, blue) colors (2022, p. 224).

Her research in analyzing digital photography of injector nozzle deposits gives insight into the fact that segmentation is only as accurate as the contrast between RGB colors in the original image. Therefore, if the variance between different subjects is small, segmentation may not result in optimum binary images, causing a greater need for preprocessing. In the case of our two-dimensional axisymmetric and planar contour plots, the image is largely separated into white, yellow, and purple, thus increasing the segmentation accuracy. There remains only a slight hindrance in the ability to threshold as the yellow wave contains a thin orange and pink outline. The thickness of this outline (along with the jaggedness of the outline) is determined by the underlying CFD simulation's 1) interfacial reconstruction method and 2) computational mesh density. In this case, the interfacial reconstruction method is PLIC, which is the most rigorous currently commercially available, while the mesh is the "ADA1" version for this project which is

relatively coarse. However, this outline is only about 10 pixels in thickness, not providing cause enough for concern over the accuracy of binarization.

Effectiveness of Edge Smoothing

The mathematical operations involved in smoothing jagged edges can often cause slight changes in data accuracy. Edge smoothing produces further data smearing and lack of preciseness in certain regards when compared to the unedited original. The effectiveness of the chosen smoothing process must remain within an acceptable percent difference from the original image to provide results that are validated and useful for adding to the field. To determine the accuracy of the results of smoothing, we chose five images at random from the directory to analyze. We then applied all steps of necessary averaging to smooth the edges (i.e. 1. Gaussian filter, 2. histogram equalization, 3. morphological opening), using a Sigma of 7 and disk structuring element of 7 connectivity with each of the five images and then segmented them. Simultaneously, a binarized image was produced from the unsmoothed original image, requiring no additional preprocessing. Immediately, we notice a stark difference in the values for segmentation that isolate the bulk of the liquid wave, with the unsmoothed image range including pixels from 200-225 intensities, while the smoothed ranges from 150-216. While this fact may not insist on the presence of infractions, it demands that the pixel distribution remains the same for purposes of the effectiveness of the methods used. When comparing the percent difference in wave heights at different points along the wave between the five unsmoothed binary images and the smoothed counterparts, we found a 1.27% to 8.53% difference. This difference translates to a discrepancy of 0.01 to 0.09 mm. The percent difference from the unsmoothed images will decrease as the Sigma decreases and with alternative structuring

element areas. We will revisit various parameters later by comparing the statistical results from entire datasets.

Wave Height Measurement Results

A numerical database of the change in the waves' height over time helps us anticipate if two-dimensional slices can substitute the large computing requirement that a three-dimensional model has. To do this, we compared maximum, minimum, standard deviation, average wave height values, and percent differences for various sections of the beach between three directories. The percent difference was calculated based on the variation between each of the 2D directories and the 3D directory. These included a 1000-frame axisymmetric slice, a 1000-frame planar slice, and the 459-frame thin 3D model slice for comparison. We performed four separate groupings of comparisons from which to evaluate the similarity to the 3D model. These included evaluating the beginning of the beach with high smoothing intensity through both global and cropped focuses and a global view of the middle of the beach through high and low Sigma values. The segmentation threshold chosen to isolate the liquid after histogram equalization was 150 – 216 for all three directories, to keep the data more normalized when comparing. We define a high smoothing intensity to be a Sigma value of 7 complemented by structuring element connectivity of 7, while a low smoothing intensity involves a Sigma of 2 and a connectivity of 4. We performed batch processing for the first grouping under the following conditions. See Table 1. This grouping served the purpose of being a control from where we were able to correlate the changes in results. Since each of the directories represents a different period and consequently has a different length of time between frames, the 2DP and 3D data were interpolated to match the sampling rate of 2DA (which had the highest sampling rate). The 2DP directory was

interpolated by a factor of 1.33 and the 3D by a factor of 1.02. To verify the accuracy of the interpolation step, we reperformed the average, standard deviation, max, and min formula of the interpolated data and compared it to the original. See Table 2. All three directories could then be plotted on the same time axis, as each unit of time was normalized. See Figure 4.

Table 1

Global High Sigma Beginning Inputs

	2DA	2DP	3D
Segmentation Threshold	150-216	150-216	150-216
Y-Shelf Value	790 px	790 px	1127 px
Sigma	7	7	7
Connectivity	7	7	7
Sensitivity	1750 px	1750 px	1750 px
Column	779 px	779 px	825 px
Beach Length	778-1012 px	778-1012 px	824-1111 px

Table 2

Global High Sigma Beginning Comparison

	2DA	% Difference	2DP	Interpolated DP	% Difference	3D	Interpolated 3D
Average	1.77	-32.0%	1.35	1.35	-48.2%	2.61	2.61
Std. Dev.	0.77	24.4%	0.64	0.64	3.0%	0.62	0.62
Max	4.10	-2.9%	3.19	3.19	-24.4%	4.22	4.07
Min	0.91	-44.5%	0.64	0.64	-60.9%	1.64	1.64

Figure 4

Global High Sigma Beginning Graph

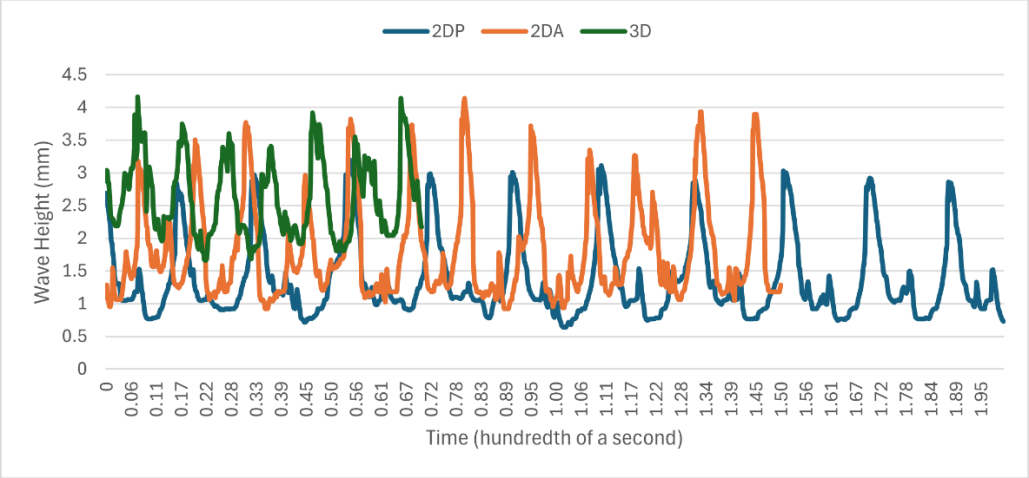

A menial hypothesis was made assuming a small data change may occur when choosing a crop area for each image before performing the processes of smoothing. This theory was tested with the second grouping of measurements, where each directory was cropped before smoothing with the continued higher Sigma and beginning beach evaluation. Since 2DA and 2DP are recorded with the same focal length, the cropping area remained the same between both. See Figure 5. The inputs used and results of cropping before smoothing are tabled below; see Table 3, Table 4, and Figure 6.

Figure 5

2DA/2DP Cropping Area

Note. Rectangular box indicates crop

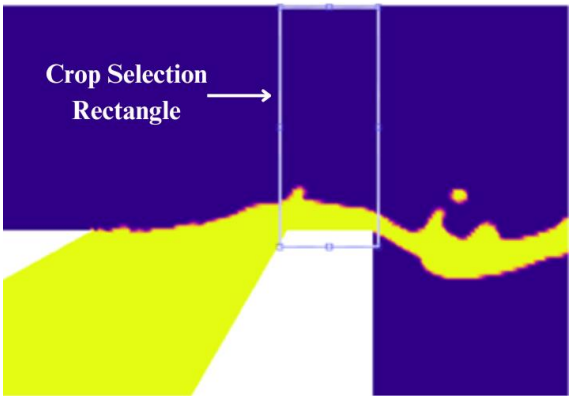

Table 3

Cropped High Sigma Beginning Inputs

	2DA	2DP	3D
Segmentation Threshold	150-216	150-216	150-216
Crop	268 x 654 px	268 x 654 px	330 x 802 px
Y-Shelf	615 px	615 px	763 px
Sigma	7	7	7
Connectivity	7	7	7
Sensitivity	1750 px	1750 px	1750 px
Column	29 px	29 px	35 px
Beach Length	778-1012 px	778-1012 px	824-1111 px

Table 4

Cropped High Sigma Beginning Comparison

	2DA	% Difference	2DP	Interpolated DP	% Difference	3D	Interpolated 3D
Average	1.79	-32%	1.36	1.36	-48%	2.61	2.61
Std. Dev.	0.76	26%	0.61	0.61	2%	0.60	0.59
Max	4.14	-4%	3.23	3.20	-25%	4.31	4.16
Min	0.92	-44%	0.64	0.64	-61%	1.66	1.66

Figure 6

Cropped High Sigma Beginning Graph

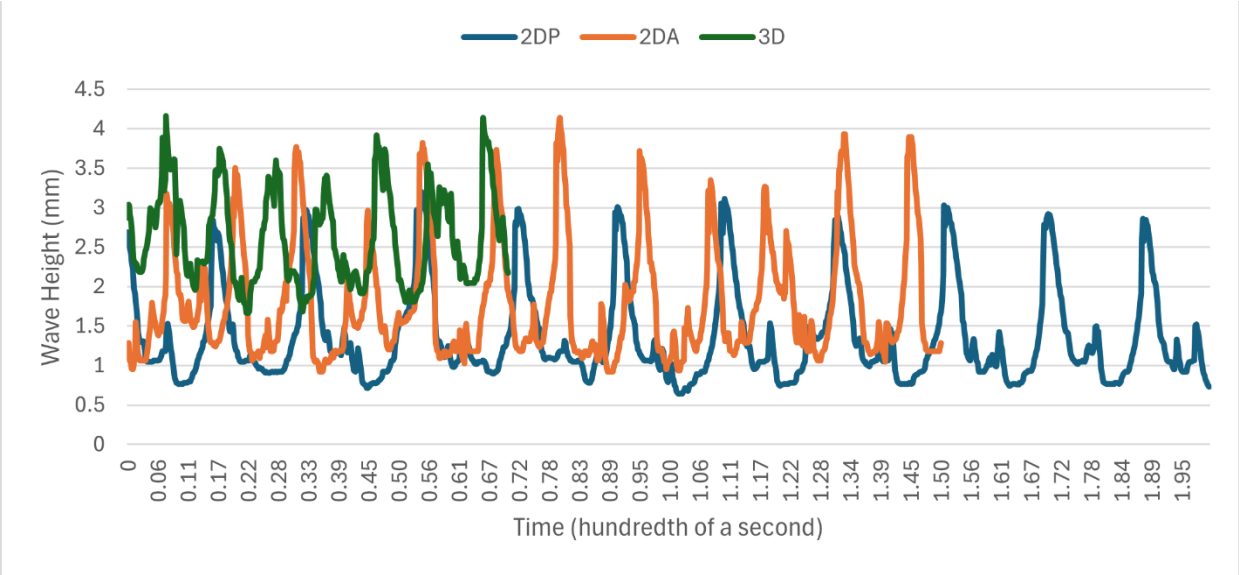

We then evaluated the middle of the beach in each of the directories to determine if a different section of the wave would show any differences in similarity to 3D through global methods. This consisted of finding half of the difference between edge abscissa values on the beach shelf from 2DA, 2DP, and 3D to ensure that we had uniformity of area of analysis. This grouping of inputs was proposed while also defining a Sigma value of 7. See Table 5. The results and interpolated graph were also exported. See Table 6 and Figure 7.

Table 5

Global High Sigma Middle Inputs

	2DA	2DP	3D
Segementation Threshold	150-216	150-216	150-216
Y-Shelf Value	790 px	790 px	1127 px
Sigma	7	7	7
Connectivity	7	7	7
Sensitivity	1750 px	1750 px	1750 px
Column	895 px	895 px	968 px
Beach Length	778-1012 px	778-1012 px	824-1111 px

Table 6

Global High Sigma Middle Comparison

	2DA	% Difference	2DP	Interpolated DP	% Difference	3D	Interpolated 3D
Average	1.77	-36%	1.32	1.32	-52%	2.77	2.77
Std. Dev.	0.97	33%	0.88	0.87	19%	0.73	0.72
Max	4.74	-1%	3.94	3.93	-18%	4.81	4.79
Min	0.68	-51%	0.44	0.44	-68%	1.38	1.38

Figure 7

Global High Sigma Middle Graph

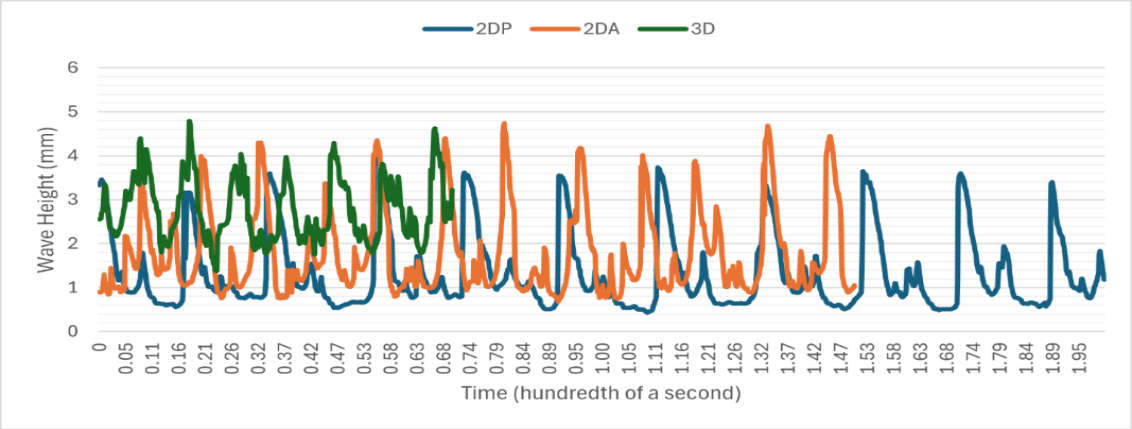

The final experiment grouping of data inputs and analysis involved executing a lower smoothing intensity with a Sigma value of 2 and structuring element connectivity of 4 also looking at the middle of the shelf. The minimum connectivity was also lowered to mirror the intent of investigating the effects of applying fewer alterations to the wave. The results are included in Tables 7, 8, and Figure 8.

Table 7

Global Low Sigma Middle Inputs

	2DA	2DP	3D
Segmentation Threshold	150-216	150-216	150-216
Y-Shelf Value	786 px	786 px	1123 px
Sigma	2	2	2
Connectivity	4	4	4
Sensitivity	750 px	750 px	750 px
Column	895 px	895 px	968 px
Beach Length	778-1012 px	778-1012 px	824-1111 px

Table 8

Global Low Sigma Middle Comparison

	2DA	% Difference	2DP	Interpolated 2DP	% Difference	3D	Interpolated 3D
Average	1.80	-36%	1.38	1.38	-51%	2.80	2.80
Std. Dev.	0.99	29%	0.91	0.89	19%	0.77	0.75
Max	4.78	0%	3.92	3.92	-18%	4.80	4.77
Min	0.68	-50%	0.46	0.46	-66%	1.37	1.37

Figure 8

Global Low Sigma Middle Graph

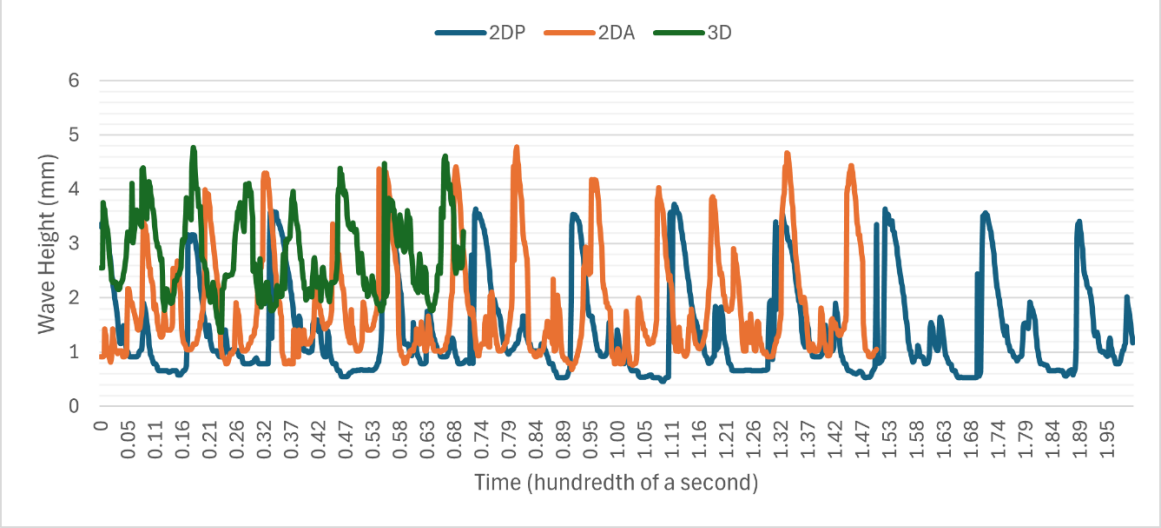

Discussion

Here, we examine the results of the change in the bulk liquid wave height over time at the exit of the neck of the nozzle atomizer, indicated by the leftmost section of the part of the simulation identified as the beach. Researchers Sikka et al. (2021) also found that looking into the "bursting phenomenon (at the neck region) effect was observed in both kinds of atomizers, which can lead to the radial dispersion of the ligaments/globules" (p. 12). Considering the definition of the length of the beach shelf that sees the motivation of the bulk wave formation, we initially define a column area of focus 1 pixel from the leftmost x-value of the beach. This area includes the exit of the slurry from the neck of the nozzle atomizer, indicating the beginning of the dispersion of droplets. See Figure 9. When considering the data, there appear to be pieces of useful information that each slice (eg. 2DA, 2DP) adds clarity to concerning the three-dimensional reality. When comparing the effect of cropping to a focus of the liquid's movement directly over the beach section before smoothing, we only interpreted an accuracy difference of 6.09342E-6% (3D minimum wave height) to 4.04% (3D maximum wave height). Thus, we have determined that the effects of cropping are not great enough to include in the batch processing for our focus herein. The control experiment encompassing the initial exit of

Figure 9

(Wilson & Strasser, 2022)

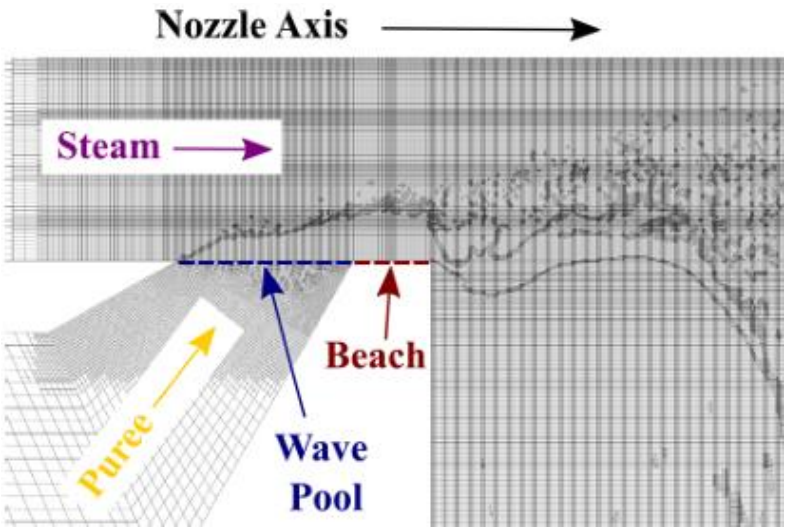

the slurry wave from the nozzle served to base our contrasting middle-beach analyses. As such, we can justify that minimal variations are seen, with only about a 1% difference decrease seen between 2DA max and 3D max in the middle beach. Many of the mathematical formulae run proved to be further from 3D when analyzing the middle of the shelf. Furthermore, we studied the impact that lowering the Sigma intensity and morphological element average in the final experiment of the middle beach. When looking for the similarity between 2DA and 3D and 2DP and 3D with a lowered smoothing application, we find that in many of the tests, there are either no differences (2DP standard deviation and max) or slightly lower percent differences (2DA standard deviation and maximum). The axisymmetric view of the wave seems to account best for estimating the maximum height reached throughout the oscillations, with a percent difference of 2.88%. Alternatively, the planar view of the fluid simulation estimates the standard deviation of wave peaks best, reflecting a percent difference of 2.90%.

Limitations

If simulation slices result in contour plots with noise and or holes, there currently exists no tools in this application for dealing with these problems during the phase of image analysis preprocessing. Thus, when processing the segmented and binarized images, corruption of accurate results may occur because of extraneous details in the noise or holes. The segmentation is simple in these directories as all of them share the same color grading scheme. As such, it has been necessary to close MATLAB and restart it to get the application or pop-up images to display correctly. Wu et al. (2020) also researched the three-dimensional distribution of atomized spray with physical models, comprised of a high-speed camera setup and computer-controlled feeds of liquid and gas. As they describe in the findings, “accurately moving the atomizer via the

3D motorized translation stage, half of the swirling atomization field can be covered, and this is large enough to reflect the quantitative features of atomization field since the swirling atomization is rotational symmetry around the swirl axis" (p. 4). As they begin to describe, the complications of measuring the complete three-dimensional properties of fluid atomization involve much finagling. Not only so, but we were unable to completely evaluate the implications of mathematical differences between wave heights for each directory, and therefore the similarities between them. The rotational symmetry can only be partially represented in our directories of axis-symmetric slices, which flatten the behavior of slurry to a two-dimensional plane.

Additionally, accounting for the effects of the steps used in the smoothing formula beforehand results in a slight shifting of the beach positions from the original, causing a reconsideration of wave measurement locations. However, this only occurs in the slightest, resulting in a once completely flat beach to have dips of 1 or 2 pixels below that which was originally positioned. When testing the accuracy of the smoothing methods comparatively to the original un-smoothed segmented image, we randomly selected 5 images from each directory and measured the wave height at a point. We evaluated a difference of 1.27% to 8.53%, largely based on the variable effects of the Gaussian filter on masses of different sizes. Not only so, but it is possible that the sensitivity threshold may have removed desirable data for a few frames within the 1000.

The differing sampling rates that each of the directories has necessitates the normalization of the time axis for all three to properly be plotted on the same graph. There are alternative methods for accomplishing this, but we chose to use interpolation to effectively

increase 2DP and 3D to the highest sampling rate found in 2DA. Through these processes, the data is averaged, estimated, and stretched to replicate the length of time represented by 1 frame of 2DA's recording. 2DP was lengthened by 330 frames, thus requiring a high level of growth estimates for the data stretching. This causes the data to be less accurate to the original values and overall behavior, but still within a 2% difference from original measurements in most cases. As a result, when viewing and measuring the amount of correlation between the directories, we have slightly decreased accuracy when plotting.

Conclusion

Summary of Findings

We were able to successfully establish a new image analysis application through MATLAB's resources to perform image analysis, preprocessing, and measurement to accomplish various purposes. Through this, a user can establish and test different segmentation thresholds to focus on information within an image. Afterward, batch processing quickly evaluates and applies all user-chosen functions and values to all files in a chosen directory. The batch processing coupled with smoothing abilities kept the data within 1.27% - 8.53% of the original binarized height measured with pixelated edges. The data can then be exported into an Excel file for storage and comparison purposes. We found somewhat significant changes in standard deviation, maximum, and minimum height when isolating different sections of the beach shelf for height measurement. Four main controls allowed us to manipulate the evaluation of the similarity between wave directories, including the column, average strel size, Sigma intensity, and lowest connectivity the user defines. Column selection determined at which abscissa the application would capture frame wave height values. The average strel size defined

the size of the structuring element that was used for morphological opening, thus affecting the reduction of edge extension caused by smoothing. The intensity of the Sigma value changed the amount of smoothing through Gaussian blurring that was applied to the RGB image. The minimum connectivity determined how large an area of true pixels grouped could be without removal, thus allowing for small bubbles to be eliminated from the segmentation. While cropping was an additional capability to confine the shelf area before applying smoothing, it proved to not have an effect significant enough to warrant usage. Ultimately, 2DA appeared to have a closer representation of 3D as seen by many of the maximum height measurements which even came to as close to 0% difference. From these analyses alone, we cannot determine whether the 2DA and 2DP counterparts can adequately represent the 3D fluid simulation due to differences in mismatched wave troughs and peaks. However, the current simplistic evaluation suggests that 2DA and 2DP are more dissimilar than similar to 3D.

Implications

Directly, achieving satisfactory results makes a breakthrough in the processing times of computational fluid dynamics, where two-dimensional slices can be produced and evaluated via image analysis batch processing giving insight into the entire three-dimensional atomization. This would allow for leaps and bounds to be made in the field at a faster rate. We propose that further research be done to estimate the ability to utilize and grow the batch processing methods to other areas of wave measurement. This can include the evaluation of independent frame beach height averaging measurements, burst width, trip trajectory (is it parabolic), and sheet thickness before bursting. Furthermore, to best interpret the similarity of growth rates and other structural predictors of 2D-axisymmetric and planar to 3D, we suggest a future utilization of dynamic time

warping. This is needed to better address what the differences in data indicate between directories. This processing mechanism helps remove differences that are created due to alternate recorded time lengths and shifts in wavelength that occur over time. A simpler approach to a likewise end could include writing a loop to shift the data 1 frame at a time and calculate the correlation coefficient between sets of data, storing the highest correlation achieved. To maximize image analysis benefits, it may be most promising to push the current research that we have performed to write and train a deep learning convolutional neural network to accomplish computer vision. This would help “look for models that can recognize patterns in images or videos and classify new images or videos into existing categories with minimum human supervision” as researchers Li et al. perform (2020, p. 14). The results found through the implication of a form of artificial intelligence in the use of computer vision to evaluate the data produced by simulations of desired phenomena were incredibly promising.

References

Akinyemi, O. S., Qavi, I., Taylor, C. E., & Jiang, L. (2023). Effect of the air-to-liquid mass ratio on the internal flow and near-field spray characteristics of a two-phase swirl burst injector. Journal of Aerosol Science, 167, 106092. https://doi.org/10.1016/j.jaerosci.2022.106092

Choi, D., Byun, J., & Park, H. (2022). Analysis of liquid column atomization by annular dual-nozzle gas jet flow. Journal of Fluid Mechanics, 943https://doi.org/10.1017/jfm.2022.435

Dang, W., Zhao, W., Schoegl, I., & Menon, S. (2020). A small-volume, high-throughput approach for surface tension and viscosity measurements of liquid fuels. Measurement Science & Technology, 31(9), 95301. https://doi.org/10.1088/1361-6501/ab8b23

Jackiw, I. M., & Ashgriz, N. (2023). Aerodynamic droplet atomization model (ADAM). Journal of Fluid Mechanics, 958https://doi.org/10.1017/jfm.2022.1046

Jüngst, N., Smallwood, G. J., & Kaiser, S. A. (2022). Visualization and image analysis of droplet puffing and micro-explosion in spray-flame synthesis of iron oxide nanoparticles. Experiments in Fluids, 63(3)https://doi.org/10.1007/s00348-022-03411-y

Khalid, A., Jaat, N., Hushim, M. F., Manshoor, B., Zaman, I., Sapit, A., & Razali, A. (2017). Computational fluid dynamics analysis of high injection pressure blended biodiesel. IOP Conference Series: Materials Science and Engineering, 226(1), 12002. https://doi.org/10.1088/1757-899X/226/1/012002

Lefebvre, A. H. (2008). ATOMIZATION. In Begellhouse eBooks. https://doi.org/10.1615/atoz.a.atomization

Li, H., Cryer, S., Acharya, L., & Raymond, J. (2020). Video and image classification using atomisation spray image patterns and deep learning. *Biosystems Engineering, 200,* 13-22. https://doi.org/10.1016/j.biosystemseng.2020.08.016

Minko, A., Guskov, O., Arefyev, K., & Saveliev, A. (2021). Physical and mathematical modeling of the interaction of water droplets and high-speed gas flow. *Applied Sciences, 11*(23), 11146. https://doi.org/10.3390/app112311146

Monieta, J. (2022). Application of image color analysis for the assessment of injector nozzle deposits in internal combustion engines. *SAE International Journal of Fuels and Lubricants, 15*(2), 221. https://doi.org/10.4271/04-15-02-0010

Mostert, W., Popinet, S., & Deike, L. (2022). High-resolution direct simulation of deep water breaking waves: Transition to turbulence, bubbles and droplets production. *Journal of Fluid Mechanics, 942*(A27)https://doi.org/10.1017/jfm.2022.330

Oswald, W., Lauk, J., Gödeke, L., Ehrhard, P., & Willenbacher, N. (2019). Analysis of paint flow pulsations during high-speed rotary bell atomization. *Coatings (Basel), 9*(10), 1-9. https://doi.org/10.3390/coatings9100674

Radcliffe, A. J., & Reklaitis, G. V. (2021). Automated object tracking, event detection, and recognition for high-speed video of drop formation phenomena. *AIChE Journal, 67*(8), n/a. https://doi.org/10.1002/aic.17245

Sikka, R., Vågsæther, K., Bjerketvedt, D., & Lundberg, J. (2021). Experimental study of primary atomization characteristics of sonic air-assist atomizers. *Applied Sciences, 11*(21), 10444. https://doi.org/10.3390/app112110444

Wilson, D. M., Strasser, W., & Prichard, R. (2023). Spatiotemporal characterization of wave-augmented varicose explosions. *International Journal of Multiphase Flow, 161*, 104352. https://doi.org/10.1016/j.ijmultiphaseflow.2022.104352

Wilson, D. M., & Strasser, W. (2022). The rise and fall of banana puree: Non-Newtonian annular wave cycle in transonic self-pulsating flow. *Physics of Fluids, 34*, 073107. https://doi.org/10.1063/5.0088341

Wu, Y., Wang, L., Lin, W., Song, G., He, Y., Wu, X., Wang, Z., & Cen, K. (2021). Picosecond pulsed digital off-axis holography for near-nozzle droplet size and 3D distribution measurement of a swirl kerosene spray. *Fuel (Guildford), 283*, 119124. https://doi.org/10.1016/j.fuel.2020.119124

Zaidi, S. B. A., Grenfell, J., Airey, G., Ahmad, N., Ahmed, I., Fareed, A., & Abed, A. (2022). Application of image analysis tools in matlab to better estimate the degree of binder coverage in rolling bottles test. *Road Materials and Pavement Design, 23*(3), 601-616. https://doi.org/10.1080/14680629.2020.1834441

Zhang, J., Li, C., Rahaman, M. M., Yao, Y., Ma, P., Zhang, J., Zhao, X., Jiang, T., & Grzegorzek, M. (2023). A comprehensive survey with quantitative comparison of image analysis methods for microorganism biovolume measurements. *Archives of Computational Methods in Engineering, 30*(1), 639-673. https://doi.org/10.1007/s11831-022-09811-x